Biochemical and Structural Characterization of a Five-domain GH115-Glucuronidase from the Marine Bacterium Saccharophagus

THE JOURNAL OF BIOLOGICAL CHEMISTRY VOL. 291, NO. 27, pp. 14120–14133, July 1, 2016
Published in the U.S.A.

Biochemical and Structural Characterization of a Five-domain GH115 α-Glucuronidase from the Marine Bacterium *Saccharophagus degradans* 2-40^{T}*[S]

Received for publication, November 13, 2015, and in revised form, March 22, 2016 Published, JBC Papers in Press, April 18, 2016, DOI 10.1074/jbc.M115.702944

Weijun Wang[‡1], Ruoyu Yan[‡1], Boguslaw P. Nocek[§], Thu V. Vuong[‡], Rosa Di Leo[‡], Xiaohui Xu[‡], Hong Cui[‡], Paul Gatenholm[¶], Guillermo Toriz[¶‖], Maija Tenkanen[**], Alexei Savchenko[‡2], and Emma R. Master[‡3]

*From the [‡]Department of Chemical Engineering and Applied Chemistry, University of Toronto, 200 College Street, Toronto, Ontario M5S 3E5, Canada, the [§]Structural Biology Center, Biosciences Division, Argonne National Laboratory, Argonne, Illinois 60439, the [¶]Department of Chemistry and Chemical Engineering, Wallenberg Wood Science Center and Biopolymer Technology, Chalmers University of Technology, Kemivägen 4, Gothenburg 412 96, Sweden, the [‖]Department of Wood, Cellulose and Paper Research, University of Guadalajara, Guadalajara 44100, Mexico, and the **Department of Food and Environmental Sciences, University of Helsinki, P.O. Box 27, Helsinki 00014, Finland*

Glucuronic acid (GlcA*p*) and/or methylglucuronic acid (MeGlcA*p*) decorate the major forms of xylan in hardwood and coniferous softwoods as well as many cereal grains. Accordingly, the complete utilization of glucuronoxylans or conversion to sugar precursors requires the action of main chain xylanases as well as α-glucuronidases that release the α- (1→2)-linked (Me)GlcA*p* side groups. Herein, a family GH115 enzyme from the marine bacterium *Saccharophagus degradans* 2-40^{T}, SdeAgu115A, demonstrated activity toward glucuronoxylan and oligomers thereof with preference toward MeGlcA*p* linked to internal xylopyranosyl residues. Unique biochemical characteristics of NaCl activation were also observed. The crystal structure of SdeAgu115A revealed a five-domain architecture, with an additional insertion C^{+} domain that had significant impact on the domain arrangement of SdeAgu115A monomer and its dimerization. The participation of domain C^{+} in substrate binding was supported by reduced substrate inhibition upon introducing W773A, W689A, and F696A substitutions within this domain. In addition to Asp-335, the catalytic essentiality of Glu-216 was revealed by site-specific mutagenesis. A primary sequence analysis suggested that the SdeAgu115A architecture is shared by more than half of GH115 members, thus defining a distinct archetype for GH115 enzymes.

The xylan backbone consists of β-(1→4)-linked D-xylopyranosyl (Xyl*p*)[4] residues, which, depending on the source, can be partially substituted at O-2 positions and/or O-3 positions with α-L-arabinofuranosyl (Ara*f*) and acetyl substituents and at O-2 positions with α-D-glucuronic acid (also called glucopyranosyluronic acid, GlcA*p*) or 4-*O*-methyl GlcA*p* (MeGlcA*p*) (1–3). Whereas glucuronoxylan is the predominant form of xylan in dicots, such as hardwoods, xylan from conifers (softwoods) contains both (Me)GlcA*p* and Ara*f* substituents (4). Xylan from monocots (*e.g.* cereals and grasses) resembles softwood xylan, although with varying (Me)GlcA*p* and Ara*f* contents. Consistent with the structural diversity of xylans, their complete enzymatic hydrolysis typically requires the concerted action of several enzymes, including endoxylanases and β-xylosidases, which target glycosidic linkages within the xylan backbone, along with α-glucuronidases, α-L-arabinofuranosidases, acetyl xylan esterases, feruloyl esterases, and glucuronoyl esterases, which target the branching substituents present in different xylan types (5–8). In addition to enabling the complete conversion of xylan to monosaccharides for digestion or utilization as biochemical precursors, debranching enzymes can be used to fine tune xylan solubility, rheology, and adherence to other biopolymers (9). In this way, α-glucuronidases may also be useful tools in the development of xylan-derived polymers with desired characteristics (10, 11).

To date, α-glucuronidases (EC 3.2.1.131/139) have been classified into three glycoside hydrolase (GH) families, namely GH4, GH67, and GH115, in the CAZy database (12). Whereas two family GH4 α-glucuronidases from *Thermotoga maritime* (TM0434 and TM0752) hydrolyze *p*-nitrophenyl-α-D-glucuronopyranoside (*p*NP-GlcA*p*), both lack activity toward 4-*O*-methyl-D-glucuronoxylan (13, 14); TM0752 also lacks activity toward aldouronic acids (13), whereas TM0434 activity toward aldouronic acids has not been tested. By contrast, α-glucuronidases from families GH67 and GH115 target the α-(1→2)-linkage between (Me)GlcA*p* and Xyl*p* of xylan and/or corresponding oligosaccharides (15–17). However, GH67 activity is restricted to (Me)GlcA*p* substituents at the non-reducing end of the substrate, presumably due to the rather deep active site pocket adopted by this enzyme family (18–21). Most of the

* This work was supported by the Government of Ontario through the project "Forest FAB: Applied Genomics for Functionalized Fibre and Biochemicals" (Grant ORF-RE-05-005 to E. R. M.). The authors declare that they have no conflicts of interest with the contents of this article.

[S] This article contains supplemental Table S1 and Fig. S1.

The atomic coordinates and structure factors (code 4ZMH) have been deposited in the Protein Data Bank (http://wwpdb.org/).

[1] Both authors contributed equally to this work.

[2] To whom correspondence may be addressed. Tel.: 416-978-3925; Fax: 416-978-8605; E-mail: alexei.savchenko@utoronto.ca.

[3] To whom correspondence may be addressed. Tel.: 416-946-7861; Fax: 416-978-8605; E-mail: emma.master@utoronto.ca.

[4] The abbreviations used are: Xyl*p*, D-xylopyranosyl; GlcA*p*, glucuronic acid (glucopyranosyluronic acid); MeGlcA*p*, methylglucuronic acid (4-*O*-methyl glucopyranosyluronic acid); *p*NP-GlcA*p*, *p*-nitrophenyl-α-D-glucuronopyranoside; *p*NP, *p*-nitrophenyl; XOS, xylooligosaccharides; Ara*f*, α-L-arabinofuranosyl; PDB, Protein Data Bank.

characterized α-glucuronidases from family GH115, on the other hand, are able to remove (Me)GlcA*p* from both terminal and internal Xyl*p* units in xylan and xylooligomers (16, 17, 22, 23) and so may be particularly beneficial to efforts aimed at harnessing xylan as a polymer. Moreover, the recent characterization of BtGH115 from *Bacteroides thetaiotaomicron* (24) supports earlier predictions that GH115 is a polyspecific enzyme family (23), given the action of BtGH115 on terminal 4-*O*-methyl-glucuronic acid residues from internal positions of arabinogalactan but not glucuronoxylan (24).

At present, more than 300 GH115 sequences are recorded in the CAZy database; however, only five representatives have been characterized to date, including the first one from *Schizophyllum commune* (ScAgu115A) (16, 22) as well as PsAgu115A from *Pichia stipitis* (now *Scheffersomyces stipitis*) (17), SpAgu115A from *Streptomyces pristinaespiralis* (25), BoAgu115A from *Bacteroides ovatus* (23) and BtGH115A from *B. thetaiotaomicron* (24). ^{1}H NMR analysis of two GH115 α-glucuronidases from *P. stipitis* and *S. commune* confirmed that, like GH67 enzymes, α-glucuronidases from GH115 adopt an inverting catalytic mechanism (26). The first crystal structure of a GH115 enzyme was reported in 2013. In their study, Bolam and co-workers (23) showed that BoAgu115A from *B. ovatus* forms a tight dimer with each monomer composed of four distinct domains (A–D). The dimerization interface comprises interactions between helical bundles of C domains in each protomer and reciprocally between the C-terminal β-sandwich (domain D) of protomer 1 and the TIM barrel of protomer 2 (domain B′) (23). The BoAgu115A-GlcA*p* complex structure allowed these authors to localize the enzyme's active site to the deep pocket within the TIM barrel domain (B/B′) of each protomer. Mutagenesis analysis demonstrated the important role of several residues, including Asp-206, Asp-332, or Glu-375, as candidates for catalytic residues and Arg-328 involved in substrate recognition. Notably, the overall structures of the first three domains of BoAgu115A bear distant evolutionary similarity with corresponding domains in GH67 enzymes, and although catalytic residues identified in each of these CAZy families do not directly align, they are all located at the C-terminal end of domain B. More recently, the BtGH115A structure revealed a four-domain architecture similar to that of BoAgu115A; however, the position of C-terminal domain D was altered and placed atop of domain C (24). Although representing the first two molecular images of GH115 family enzymes, the structural insights gained to date cannot be directly applied to more than 50% GH115 members due to a substantial sequence insertion, thus necessitating further studies of corresponding GH115 representatives.

Saccharophagus degradans 2-40^T is an aerobic marine bacterium that can degrade several complex polysaccharides, including agar, chitin, alginic acid, carrageenan, cellulose, β-glucan, laminarin, pectin, pullulan, starch, and xylan (27–29). The *S. degradans* 2-40^T genome sequence was reported in 2008 and was found to encode at least 128 carbohydrate active enzymes relevant to polysaccharide hydrolysis (30). In particular, for xylan utilization, the genome sequence revealed several genes encoding GH10 and GH11 endoxylanases as well as genes encoding xylan debranching enzymes, including α-L-arabinofuranosidases from families GH43 and GH51, acetyl xylan esterases from families CE1 to CE3, and α-glucuronidases from families GH67 and GH115 (31).

To further map the diversity of GH115 family enzymes, we undertook a detailed biochemical and structural characterization of the GH115 α-glucuronidase from *S. degradans* 2-40^T (SdeAgu115A), which shares <40% sequence identity with previously characterized GH115 representatives (33% with BoAgu115A, 39% with PsAgu115A, 38% with ScAgu115A, and 23% with BtGH115A). The crystal structure of the SdeAgu115A monomer revealed five distinct domains, in contrast to the four-domain composition of BoAgu115A and BtGH115A (23, 24), resulting from the insertion of an additional 125-amino acid domain between domains C and D, herein referred to as C$^+$. Detailed structural and mutagenesis studies of SdeAgu115A demonstrated the role of domain C$^+$ in domain arrangement, enzyme dimerization, and substrate binding; Glu-216 in SdeAgu115A was also identified as an essential catalytic residue. Finally, biochemical analyses using defined xylo-oligosaccharides as well as multiple xylan sources confirmed SdeAgu115A action toward α-(1→2)-glycosidic linkages between (Me)GlcA*p* and singly substituted Xyl*p* residues at both internal and terminal positions of the substrate.

Experimental Procedures

Materials—Pfx polymerase was purchased from Invitrogen. The QIAEX II gel extraction kit and QIAquick PCR purification kit were purchased from Qiagen. Phosphorylase *b* from rabbit muscle, beechwood xylan, and oat spelt xylan were purchased from Sigma-Aldrich; GH11 endoxylanase from *Neocallimastix patriciarum* and the D-glucuronic acid assay kit were purchased from Megazyme; GH10 xylanase (Shearzyme®) and GH11 xylanase (Pentopan® Mono BG) were obtained from Novozymes; *p*NP-GlcA*p* was purchased from TCI. Spruce arabinoglucuronoxylan was prepared as reported previously (32). Genomic DNA of *S. degradans* 2-40^T (ATCC catalog no. 43961) was purchased from American Type Culture Collection. All other chemicals were analytical grade and obtained from Sigma-Aldrich or Fisher.

DNA Manipulation—The gene encoding the mature form of SdeAgu115A (GenBank^{TM} accession number ABD81015) without a signal peptide (aa residues 1–32) was amplified from *S. degradans* genomic DNA with Pfx DNA polymerase (Invitrogen). The infusion cloning kit from Clontech was used to transfer purified PCR products to the p15Tv-L expression vector (GenBank^{TM} accession number EF456736), generating p15Tv-L_SdeAgu115A. Site-specific mutagenesis was carried out according to a modified QuikChange^{TM} (Stratagene) method (33). All constructs were verified by DNA sequencing at the Center of Applied Genomics at the SickKids Hospital in Toronto.

GH115 Enzyme Sequence Analysis—Enzyme sequences were retrieved from the CAZy database and the JGI fungal genomes database (November 22, 2014). The sequences were curated by removing members that had sequences shorter than 200 amino acid residues or lacked the catalytic domain B. In total, 303 GH115 α-glucuronidase sequences were collected and then aligned using MUSCLE in Geneious version 6.0.6. Geneious

Tree Builder version 6.0.6 was used to create phylogenetic tree with the neighbor-joining method.

Purification of Recombinant SdeAgu115A—Escherichia coli BL21(λDE3) codon plus strain harboring p15Tv-L_SdeAgu115A was propagated at 37 °C in 1 liter of Luria-Bertani medium supplemented with 0.5 M D-sorbitol, 2.5 mM glycine betaine, 34 μg ml^{-1} chloramphenicol, and 100 μg ml^{-1} ampicillin. At $A_{600\,nm}$ of 0.6, the cultivation temperature was reduced to 15 °C, and recombinant protein expression was induced with 0.5 mM isopropyl β-D-thiogalactopyranoside overnight.

The induced cultures were harvested by centrifugation at 6000 × *g* for 15 min. Cell pellets (~4.3 g fresh weight) were suspended in 30 ml of binding buffer (300 mM NaCl, 50 mM HEPES (pH 7.0), 5% glycerol, 5 mM imidazole) and disrupted by sonication. Cell debris was removed by centrifugation (17,500 × *g*, 20 min), and supernatants were passed through a 0.45-μm filter before being incubated for 45 min with 5.0 ml of pre-equilibrated nickel-nitrilotriacetic acid resin (Qiagen) at 4 °C. Resin was then washed with 300 ml of washing buffer (300 mM NaCl, 50 mM HEPES (pH 7.0), 5% (v/v) glycerol, 50 mM imidazole), and bound protein was eluted with ~30 ml of elution buffer (300 mM NaCl, 50 mM HEPES (pH 7.0), 5% (v/v) glycerol, 250 mM imidazole) in a stepwise manner. Active fractions were pooled and adjusted to 1.0 M NaCl before being applied to a phenyl-Sepharose™ hydrophobic interaction chromatography column (1 × 18.5 cm) equilibrated with the same buffer (50 mM HEPES (pH 7.0) containing 1.0 M NaCl). Fractions (5 ml) were collected at a flow rate of 1.5 ml min^{-1} and linear gradient of 1.0 to 0 M NaCl in 50 mM HEPES (pH 7.0) over 5 column volumes. All chromatographic steps were performed using the BIOSHOP Duoflow system (Bio-Rad). Fractions containing SdeAgu115A were exchanged to 25 mM HEPES buffer (pH 7.0) containing 300 mM NaCl using a Bio-Gel P10 column. Amicon stirred ultrafiltration cells (Millipore) equipped with a polyethersulfone membrane (nominal molecular weight 100,000) were then used to concentrate purified protein samples before aliquots were flash-frozen in liquid nitrogen and then stored at −80 °C.

Protein concentrations were determined using the Bradford assay and bovine serum albumin as a standard (34). SDS-PAGE was performed and stained with Coomassie Blue according to established procedures (35).

Production of MeGlcAp-substituted xylooligosaccharides (U^{4m2}XX and XU^{4m2}XX)—Birchwood xylan 1% (w/v) prepared in 300 ml of 50 mM sodium acetate buffer (pH 5.0) was boiled for 5 min and then cooled before the addition of endoxylanases. GH10 xylanase (Shearzyme®) (20 microkatals/g xylan) and GH11 xylanase (Pentopan® Mono BG) (30 microkatals/g xylan) were separately added to generate U^{4m2}XX and XU^{4m2}XX, respectively. Enzymatic hydrolyses were performed at 40 °C for 72 h with a continuous mixing, and the extent of hydrolysis was regularly checked by TLC. The reaction was stopped by 20-min boiling, and the supernatant was collected after a centrifugation of 15,000 × *g* for 15 min. Acidic glucuronyl xylooligosaccharides (XOS) were isolated using Dowex 1 × 2 anion exchange resin (75 ml; Sigma), which had been regenerated with 10 volumes of degassed 2 M ammonium formate (pH 6.0) and washed with 2 volumes of water in an Äkta chromatography system (GE Healthcare). Unbound neutral XOS were washed with water (1 ml min^{-1}). Bound acidic glucuronyl XOS were eluted with an 800-ml gradient of 0–400 mM ammonium formate (pH 6.0) and concentrated to 4 ml in a rotatory evaporator and further purified using BioGel-P2 size exclusion chromatography (8.9 × 135 cm; Bio-Rad) with Milli-Q water (Millipore) as the eluent. Pure sugar factions were concentrated using a rotary evaporator, and the total carbohydrates were determined by the phenol-sulfuric acid method using xylose as the standard (36). The purity was determined by TLC, high performance anion exchange chromatography with pulsed amperometric detection, and mass spectrometry using purified U^{4m2}XX and XU^{4m2}XX as the standard (37). Mass spectrometric analyses of purified XOS were performed using an Agilent XCT Plus model ion trap mass spectrometer (Agilent Technologies, Waldbronn, Germany) equipped with LC/MSD Trap Software version 5.2, as described by Vuong *et al.* (38). Hydrolysis products and chromatography fractions were analyzed with TLC on Silica Gel 60 aluminum plates (Merck, Darmstadt, Germany), which were developed in ethyl acetate/acetic acid/isopropyl alcohol/formic acid/water (25:10:5:1:15, v/v/v/v/v). The plate was sprayed with 0.2% orcinol solution in 80% ethanol (v/v) and 10% H_2SO_4 (v/v) and heated at 100 °C for 2–5 min to detect XOS.

Effect of Temperature, pH, Metal Ions, and NaCl—The thermostability of SdeAgu115A was evaluated by incubating the enzyme (300 μg/ml) at pH 6.5 in 0.2 ml of 200 mM MES for up to 4 h at 25, 35, 40, and 50 °C. Following incubation, residual activity was measured by transferring 6.0 μg of the heat-treated enzyme to a final 0.2-ml reaction mixture comprising 200 mM MES (pH 6.5) and 1.0% (w/v) beechwood xylan. After a 10-min incubation at 40 °C, reaction products were quantified using the Nelson-Somogyi assay for reducing sugars (39). The pH optimum of SdeAgu115A was determined by measuring activity as described above, this time in buffers with a pH range from 4.0 to 9.5. Buffers used were 200 mM CH_3CO_2Na (pH 4–5.5), 200 mM MES (pH 6.0–8.0), and 200 mM glycine-NaOH (pH 8.5–9.5). To determine pH stability, residual SdeAgu115A activity was measured after a 24-h incubation at 4 °C in buffers with a pH range from 4.0 to 9.5. The effect of metal ions was determined by adding 1.0 mM $CaCl_2$, $MgCl_2$, $CoCl_2$, $MnCl_2$, $NiCl_2$, $CdCl_2$, $AgNO_3$, $ZnCl_2$, $CuSO_4$, or $HgCl_2$ to the activity assay mixture.

To further investigate the impact of NaCl on SdeAgu115A activity, the enzyme was dialyzed against 100 mM MES buffer (pH 6.5) before activity measurements in 100 mM MES buffer (pH 6.5) containing 0–1.5 M NaCl.

Analytical Ultracentrifugation for Oligomeric State Analysis—Sedimentation equilibrium analytical ultracentrifugation was carried out using a Beckman Optima XL-A analytical ultracentrifuge equipped with an An-60 Ti rotor. Protein absorbance was monitored at 280 nm. Data were collected at speeds of 6000, 7000, and 8000 rpm using SdeAgu115A at varying enzyme concentrations (5.9, 3.0, and 1.5 μM) in 20 mM HEPES (pH 7.0, 300 mM NaCl) at 20 °C. Data analysis was performed using the Origin MicroCal XL-A/CL-I Data Analysis Software Package version 4.0. The density of buffer and the partial specific volumes of protein were calculated using SedNterp (40).

CD Spectra—CD was recorded with an Aviv model 202 circular dichroism spectrometer from 200 to 300 nm at 25 °C in a 0.5-cm path length cell. The spectral bandwidth was 1.0 nm, the step size was 1.0 nm, and the averaging time was 1.0 s. The protein sample was in 0.2 M sodium phosphate buffer (pH 7.5) with an adjusted concentration of 1.0 mg/ml.

Affinity Gel Electrophoresis—The binding of SdeAgu115A and its mutants (E216A and D335A) to beechwood xylan was examined by native affinity gel electrophoresis (41) with minor modifications. Briefly, the native polyacrylamide gels contained 6.0% (w/v) acrylamide in 15 mM Tris, 150 mM glycine, 100 mM sodium phosphate buffer (pH 8.8), and 0.05 and 0.1% (w/v) of the test polysaccharide. Approximately 7.0 μg of SdeAgu115A and each mutant were loaded onto the gels and then run at 70 V for 6.0 h. Relative binding affinities were inferred from the migration distance of the wild type and mutant enzymes on gels with and without the test polysaccharides. BSA and phosphorylase *b* from rabbit muscle (7.0 μg) were used as reference proteins.

Protein Crystallization, Data Collection, and Structure Determination—For crystallographic purposes, the selenomethionine-substituted protein was overexpressed using M9 high yield growth medium (Medicilon Inc.) and purified according to the above-described procedure for recombinant SdeAgu115A.

SdeAgu115A was concentrated to 13.0 mg ml^{-1} in 10 mM HEPES (pH 7.5) containing 500 mM NaCl. The crystallization screen was performed by mixing 0.5 μl of protein with 0.5 μl of reservoir buffer using a Mosquito crystal (TTPlab) liquid-handling system. The SdeAgu115A crystals were obtained by a sitting drop vapor diffusion method at 23 °C in the presence of 200 mM sodium dihydrogen phosphate, 100 mM sodium acetate (pH 4.6), 200 mM ammonium acetate, and 30% PEG 4000. The crystals were flash-frozen in liquid nitrogen using paratone-N oil as cryoprotectant. Diffraction data for SdeAgu115A crystals were collected at the Argonne National Laboratory, Structural Biology Center at the Advanced Photon Source, using beamline 19-ID with an ADSC Quantum 315R detector according to a previously described experimental set-up (42, 43). All diffraction data were processed using the HKL3000 suite of programs (44). The SdeAgu115A structure was determined by the single-wavelength anomalous diffraction method using phasing, density modification, and initial protein model building as implemented in the HKL3000 software package (45–51). Cycles of manual corrections of the model were carried out in COOT and with REFMAC of CCP4 and finalized with Phenix using the implemented TLS group refinement routine. The final model was refined against all reflections except for 5% randomly selected reflections, which were used for monitoring R_{free}. Final refinement statistics are presented in Table 1. Structure figures were prepared using PyMOL v1.3 (Schrödinger LLC, New York).

Substrate Preference and Enzyme Kinetics—SdeAgu115A activity on various xylans and xylooligosaccharides was measured using the D-glucuronic acid assay kit from Megazyme. Reactions were performed for 10 min at 40 °C and were initiated by adding 5 μl of enzyme to 20 μl of 1.0% (w/v) substrate in 200 mM MES buffer (pH 6.5). Enzyme reactions were stopped by adding 2.5 μl of 2.0 M HCl, followed by incubation at 25 °C for 10 min. NaOH (2.5 μl of a 2.0 M solution) was used to neutralize reaction mixtures before product detection. In all cases, enzyme doses were optimized to obtain initial rates of reaction. D-(+)-Glucuronic acid (0.01–1.2 mg/ml) was used to generate a standard curve.

The activity on *p*NP-GlcA*p* was determined by measuring *p*NP release. The reaction mixture contained substrate in 0.15 ml of 200 mM MES buffer (pH 6.5). SdeAgu115A doses were adjusted to obtain initial rates of reaction at 40 °C over 10 min. Reactions were terminated by adding 0.15 ml of 4% (w/v) Na_2CO_3. The amount of *p*NP formed was measured by absorbance at 405 nm, where *p*NP (50 – 400 μM) was used to generate a standard curve.

Kinetic parameters were obtained using 0.1–25 mM *p*NP-GlcA*p*, 1.0–38.4 mM $U^{4m2}XX$, and 1.0–31.9 mM $XU^{4m2}XX$. Apparent kinetic parameters for beechwood xylan were also obtained at substrate concentrations from 0.5 to 40 mg/ml. In all cases, enzyme dose was adjusted to measure initial rates of reaction at 40 °C over 10 min (0.1, 0.7, 0.7, and 140 μg of SdeAgu115A for beechwood xylan, $U^{4m2}XX$, $XU^{4m2}XX$, and *p*NP-GlcA*p*, respectively). Kinetic parameters were calculated using GraphPad version 5.0 (GraphPad Software).

Finally, mass spectrometry was used to confirm the specific release of MeGlcA*p* from beechwood xylan by SdeAgu115A. Briefly, 160 μl of 1% (w/v) beechwood xylan was incubated with 40 μl of SdeAgu115A (54 μg) in water at 22 °C for 12 h. Electrospray ionization mass spectrometric analyses were performed using a Q-Exactive mass spectrometer (Thermo Scientific) in negative mode, and product spectra were compared with D-glucuronic acid.

Results and Discussion

Sequence Analysis and General Biochemical Properties of SdeAgu115A—Multiple-sequence alignment of 303 curated GH115 sequences exhibited two main groups of GH115 enzymes that were distinguished by the presence of an amino acid insertion motif corresponding to amino acid residues 667–792 in SdeAgu115A (Fig. 1*A*). Based on sequence alignment, nearly all (97%, 94 of 97 sequences) of the fungal GH115s appeared to comprise this conserved sequence insertion motif, whereas roughly 56% (109 of 195 sequences) of bacterial sequences, including previously characterized BoAgu115A and BtGH115A enzymes, lacked the insertion. In addition to these two major forms, 11 GH115 sequences featured additional C-terminal sequences, and six GH115 enzyme sequences corresponded to only the three N-terminal domains identified in BoAgu115A. Phylogenetic analysis of GH115 sequences showed that those with the insertion motif from both fungi and bacteria were grouped together (Fig. 1*B*), further suggesting a common yet uncharacterized structural arrangement shared by these enzymes. Notably, the N-terminal sequence of SdeAgu115A revealed a secretion motif (signal peptide/signal sequence) in line with the proposed extracellular function of these enzymes.

To characterize an α-glucuronidase from the GH115 subgroup containing an insertion motif, SdeAgu115A lacking the native signal peptide sequence (residues 1–32) was expressed in

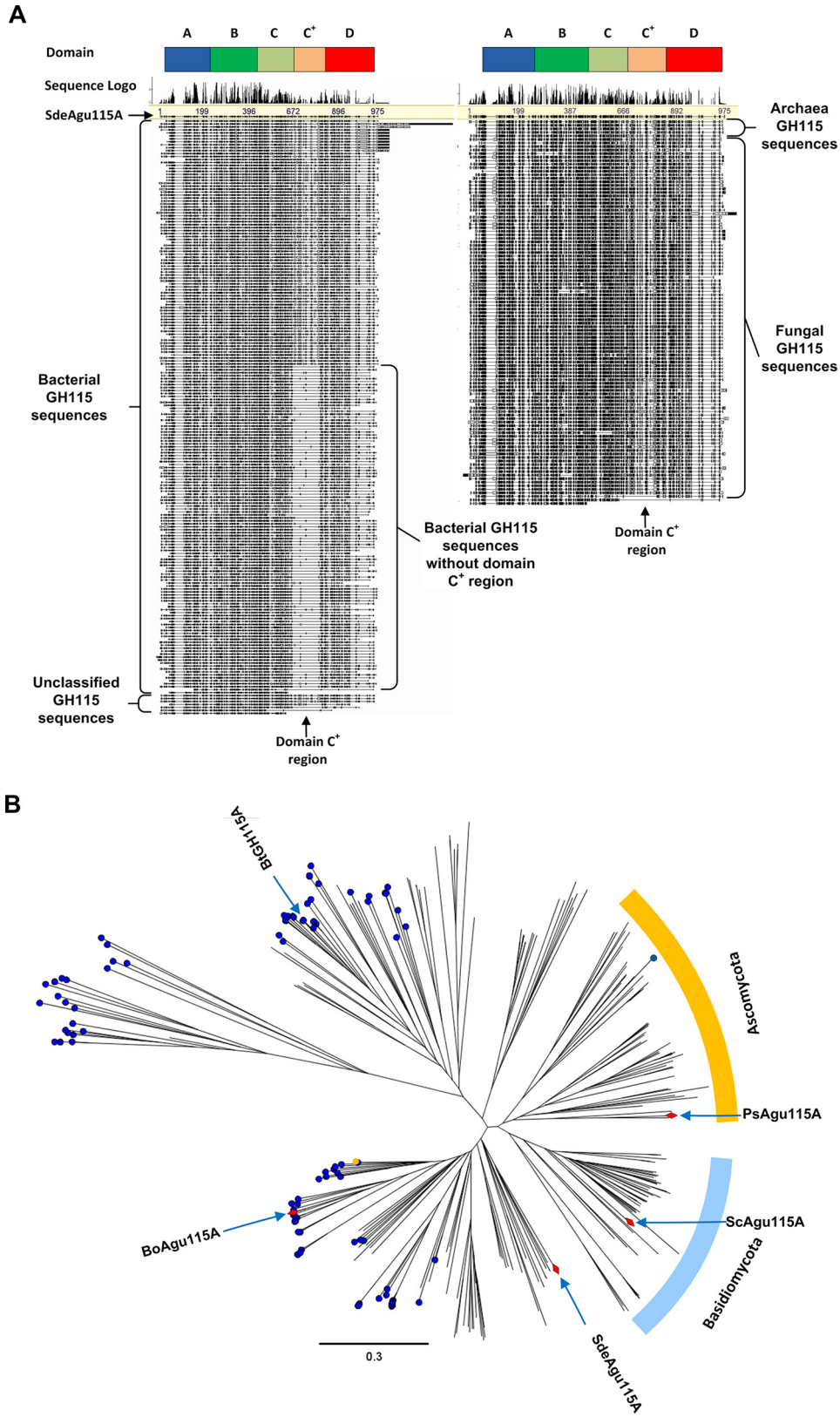

FIGURE 1. **Sequence analysis of curated GH115 α-glucuronidase sequences.** *A*, the global view of multiple-sequence alignment to display the distribution of the inserted sequence region for domain C^+ across 303 curated GH115 α-glucuronidase sequences. The amino acid sequences were retrieved from the CAZy database and the JGI fungal genomes database (November 22, 2014). All sequences were aligned using MUSCLE in Geneious version 6.0.6. *B*, phylogenetic analysis of GH115 α-glucuronidase sequences. The tree was constructed using Geneious Tree Builder version 6.0.6 and the neighbor-joining method. Enzymes predicted to comprise four domains are indicated by a *blue dot*; a *red prism* indicates biochemically characterized enzymes. In general, GH115 α-glucuronidases comprising four or five domains fall into two separate subgroups.

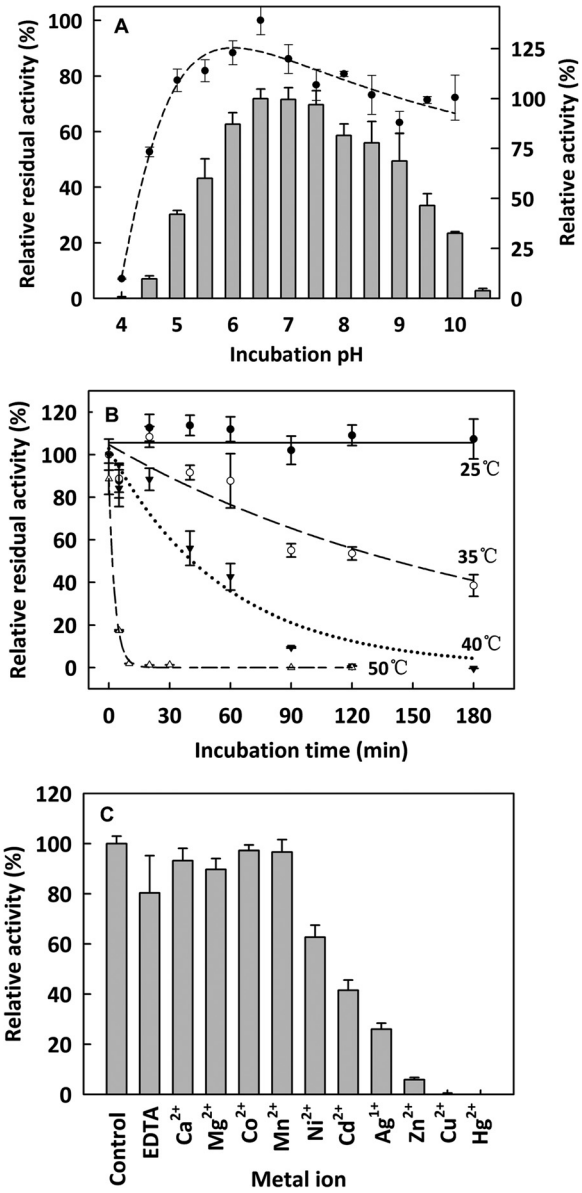

FIGURE 2. **The general properties of SdeAgu115A.** *A*, pH activity profile (*bar*) and stability (*dot*) of purified SdeAgu115A; *B*, thermostability of purified SdeAgu115A; *C*, effect of metal ions on SdeAgu115A activity. The activity assay solution contained 1.0 mM selected metal ions or 10 mM sodium EDTA. Enzyme assays were performed using 1.0% (w/v) beechwood xylan and 0.03 μg/μl SdeAgu115A. $n = 3$; *Error bars*, S.D. The specific activity value corresponding to 100% was 2470 μmol of product/min/μmol of enzyme.

E. coli in fusion with an N-terminal His tag and purified to homogeneity. The weight-average molecular mass of native SdeAgu115A was determined to be 189 ± 3.9 kDa by sedimentation-equilibrium analytical ultracentrifugation (supplemental Fig. S1), indicating that SdeAgu115A forms homodimers under the used experimental conditions (25 mM HEPES buffer (pH 7.0) containing 0.3 M NaCl). By comparison, BoAgu115A was also shown to form a stable dimer in solution (23), whereas BtGH115A appears to remain in monomeric form (24).

The SdeAgu115A activity on beechwood xylan was optimal at pH 6.5, and this recombinant enzyme retained more than 50% activity after 24-h incubation at 4 °C and pH 5.5–9.5 (Fig. 2*A*). In comparison, the optimal pH of BoAgu115A (23), ScAgu115A (16, 22), and PsAgu115 (17) was reported to be 7.0, 5.8, and 4.4, respectively. SdeAgu115A was stable for more than 3 h at 23 °C, whereas the half-life of SdeAgu115A at 35, 40, and 50 °C was ~90, 60, and 2 min, respectively (Fig. 2*B*). Whereas SdeAgu115A lost all activity after incubation at 70 °C for 5 min, PsAgu115A lost 50% activity after 30 min at 60 °C and was stable for at least 3 h at 40 °C (17). ScAgu115A retained full activity after 24 h at 40 °C between pH 6 and 8 and 65% activity after 24 h of incubation at 45 °C (16, 22).

TABLE 1
Data and refinement statistics

Data collection statistics for APS-SBC-19ID	
Space group	$P2_12_12_1$
Unit cell (Å)	
a	116.4
b	124.3
c	180.0
Resolution (Å)	38.2–1.93
Wavelength (Å)	0.9794
No. of observed reflections	204,709
No. of unique reflections	48,738
R_{pim} [a] (%)	4.0 (61.1)[b]
Completeness (%)	97.7 (96.8)
I/δ	19.1 (1.5)
Phasing	
Phasing method	SAD[c]
Refinement statistics	
R_{cryst} (%)	13.90
R_{free} (%)	16.94
Protein residues	1866
Sodium/phosphate/glycerol/acetate molecules	2/4/2/2
Solvent	2185
Root mean square deviation from target values	
Bond lengths (Å)	0.011
Bond angles (degrees)	1.22
Average *B* factors (Å^2)	
Protein	27.8
Ions	46.0
Solvent	37.8
PDB code	4ZMH
Ramachandran (%) F/A/O[d]	97/3.0/0

[a] $R_{pim} = \Sigma_{hkl}(1/(N-1)^{1/2})\Sigma_i|I_{i(hkl)} - \bar{I}hkl|/\Sigma_{hkl}\Sigma_i I_{i(hkl)}$.
[b] Numbers in parentheses are values for the highest resolution bin.
[c] Single-wavelength anomalous diffraction.
[d] As defined by MOLPROBITY (F (favored)/A (allowed)/O (outliers)).

Of the 10 ions tested, the presence of 1.0 mM Ni^{2+}, Cd^{2+}, Ag^{+}, Zn^{2+}, Cu^{2+}, and Hg^{2+} inhibited SdeAgu115A activity by ~40–100%, whereas the rest did not have any significant affect on the enzyme's activity (Fig. 2*C*). Moreover, the addition of 10 mM EDTA did not significantly affect SdeAgu115A activity, indicating that this enzyme does not strictly depend on ion supplementation for its activity under the tested experimental conditions (Fig. 2*C*). Consistently, no metal ions were observed in the crystal structure of the enzyme. The effect of metal ions on the specific activity of other GH115 enzymes has not been tested. Altogether, these data will inform optimization efforts for future enzyme applications.

Crystal Structure of SdeAgu115A Revealed an Additional Domain—The SdeAgu115A crystal structure was determined using the single-wavelength anomalous diffraction approach and selenomethionine-labeled protein. The final model of SdeAgu115A consisted of two polypeptide chains in the asymmetric unit, spanning residues 40–974 (chain A) and 40–975 (chain B). Additional density was assigned as two sodium and two phosphate ions, one glycerol, and one acetate molecule. The final model exhibited excellent crystallographic and geometric statistics, which are summarized in Table 1.

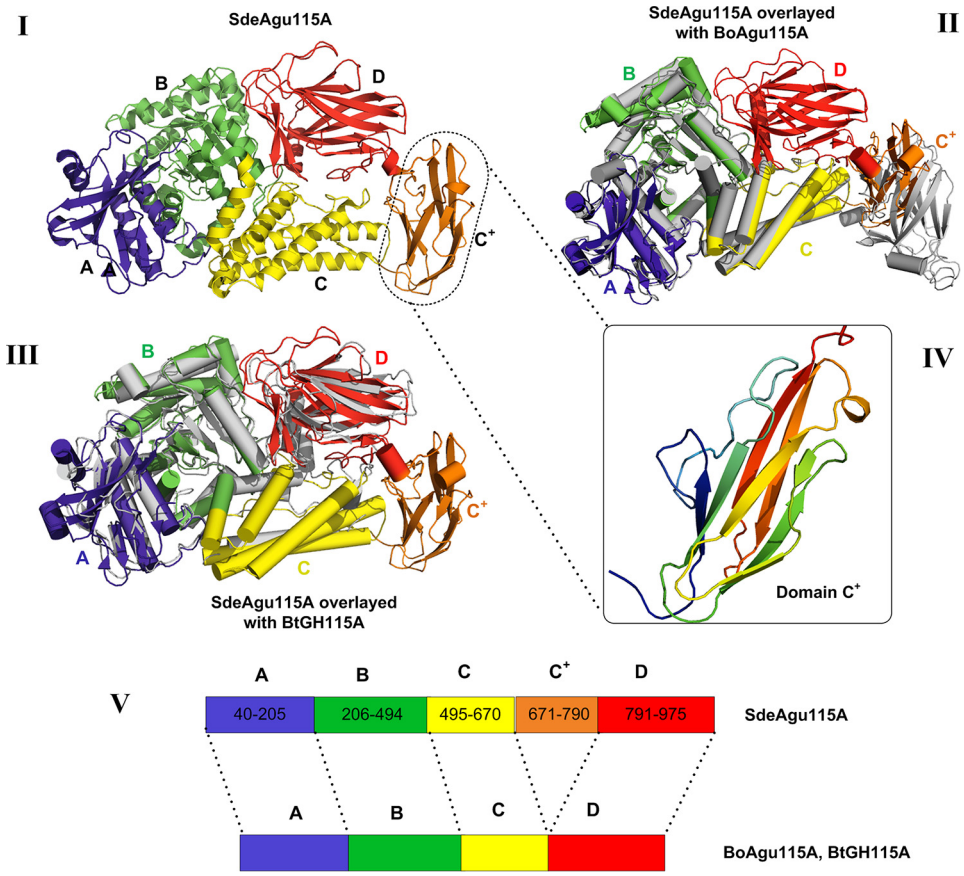

FIGURE 3. **The overall structure of SdeAgu115A, revealing a novel five-domain arrangement.** *I*, the five-domain structure of SdeAgu115A (each domain is *labeled* and *colored* for clarity: *blue* for domain A, *green* for domain B, *yellow* for domain C, *orange* for domain C^+, and *red* for domain D); *II*, SdeAgu115A overlaid with four-domain BoAgu115A shown in *gray* (helices are shown as *cylinders*); *III*, SdeAgu115A overlaid with four-domain BtGH115A shown in *gray* (helices are shown as *cylinders*); *IV*, the fold of domain C^+ (residues 671–790), displaying a β-barrel mainly consisting of eight anti-parallel β-strands; *V*, schematic drawing of the domain organization for SdeAgu115A in comparison with BoAgu115A and BtGH115A.

In contrast to previously structurally characterized GH115 enzymes (23, 24), the crystal structure of the SdeAgu115A monomer revealed a five-consecutive domain architecture with N-terminal domains A (residues 40–205), B (residues 206–494), C (residues 495–670), and the unique C^+ domain corresponding to the insertion (residues 671–790) conserved in one of two major groups within the GH115 family (Figs. 1 and 3); in SdeAgu115A, domain C^+ is then followed by the C-terminal D domain (residues 791–975).

Superimposition of SdeAgu115A with BoAgu115A and BtGH115A demonstrated a root mean square deviation of 2.4 and 2.1 Å, respectively (Fig. 3 and supplemental Table S1). Like BoAgu115A and BtGH115A, domain A of SdeAgu115A adopted a two-layer β-sandwich fold, composed of a central five-stranded β-sheet linked to a smaller two-stranded anti-parallel β-sheet between three α-helices (classified as Pfam 03648), whereas domain B displayed a distorted $(\beta/\alpha)_8$ TIM barrel fold featuring short third and fourth β-strands (classified as Pfam 15979). Domain C of SdeAgu115A comprised a five-helix bundle with a ~35-residue long loop disrupted by a short β-strand. In the case of SdeAgu115A, the five-helix bundle is wedged between domains B and C^+, whereas the loop and short strands are located at the side of this domain (Fig. 3*A*). In addition to close structural similarity to corresponding domains in BoAgu115A and BtGH115A, domains A–C in SdeAgu115A also share overall structural similarity with a GH67 α-glucuronidase from *Geobacillus stearothermophilus* (PDB code 1K9E) (20), GH84 *O*-GlcNAcase from *Clostridium perfringens* (PDB

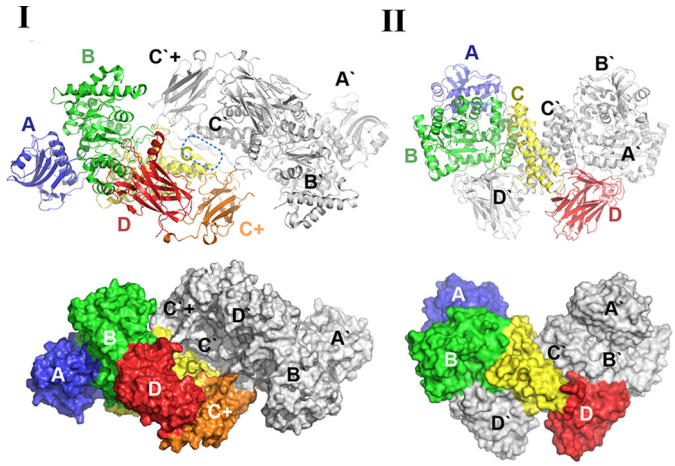

FIGURE 4. **The dimerization of SdeAgu115A in comparison with BoAgu115A.** *I*, dimerization pattern of SdeAgu115A. *II*, dimerization pattern of BoAgu115A. Side by side comparison between SdeAgu115A and BoAgu115A reveals different dimer formation schemes, which are presented in both schematic and surface forms. Each domain in protomer 1 is *labeled* and *colored* for clarity (*blue* for domain A, *green* for domain B, *yellow* for domain C, *orange* for domain C^+, and *red* for domain D), whereas all domains from protomer 2 are *colored* in *gray*.

code 2VUR) (53), and GH20 lacto-*N*-biosidase from *Bifidobacterium bifidum* (PDB code 4H04) (54) (supplemental Table S1).

Also similar to BoAgu115A and BtGH115, the C-terminal domain D of SdeAgu115A adopted a "jelly-roll" β-sandwich fold consisting of two β-sheets, each having five anti-parallel β-strands. However, the presence of the C^+ domain in SdeAgu115A significantly impacted the positioning of this domain D compared with BoAgu115A (Fig. 3) (23).

As mentioned above, domain C^+ in the SdeAgu115A structure corresponds to the additional insertion sequence, which is present in more than half of GH115 members. The C^+ domain in SdeAgu115A displayed a β-barrel composed of eight anti-parallel β-strands (Fig. 3*IV*). A structural similarity search using the Dali server (55) showed that it is most similar to the S pilus periplasmic chaperone protein SfaE (PDB code 1L4I) (56) and the chaperone protein FimC from *E. coli* (PDB code 3BWU) (57). Both proteins are involved in bacterial pilus biogenesis. More interestingly, domain C^+ is also structurally similar to the Bacon domain (Bacteriodetes-associated carbohydrate-binding often N-terminal, Pfam 13004) in BoGH5A, a GH5 endoxyloglucanase from *B. ovatus* (supplemental Table S1) (58). Bacon domains have been identified in several other carbohydrate-active enzymes as well as proteases (2704 sequences deposited in the current Pfam database) (59), suggesting that the C^+ domain in GH115 enzymes might play a role in carbohydrate binding as well as protein-protein interactions.

Distinct Domain Composition of SdeAgu115A Significantly Impacted Its Domain Arrangement and Dimerization—The overlay of SdeAgu115A (five domains) with BoAgu115A (four domains) clearly showed that insertion of the C^+ domain in SdeAgu115A impacted the position of domain D, where domain C^+ was placed at the position equivalent to the domain D in BoAgu115A and consequently shifted the domain D position to the top of domain C (Figs. 3 and 4). This change of domain composition and arrangement in SdeAgu115A prevented the enzyme from forming a butterfly-like dimer, as observed in the BoAgu115A structure (23). In BoAgu115A, the dimer is arranged by the crossing of complementary helical bundles of domain C from each promoter and is further strengthened by interactions of domain D of protomer A with domain B′ from protomer B and *vice versa* (Fig. 4*II*). In contrast, the interface of the SdeAgu115A dimer was contributed primarily through interactions between anti-parallel β-sheets and their flanking region (residues 665–670) from C domains of each protomer, which formed on the opposite side of domain C relative to domain D (Fig. 4*I*). Additional contacts between SdeAgu115A subunits were formed between the loops of the C^+ domain in protomer A and loop regions from domains C′ and B′ in the protomer B. The overall interface between two SdeAgu115A promoters covers ~1371 Å^2 according to a PDBsum/PISA server estimate (60), which corresponds to only 3.9% of each promoter surface area and involves 42 residues in each subunit. In comparison, the overall interface between BoAgu115A promoters is ~4000 Å^2 and involves 158 residues, accounting for 12.4% of each subunit surface area.

The recently determined structure of BtGH115A unveiled a second four-domain architecture for the GH115 family (24). This structure closely resembled the domain organization of

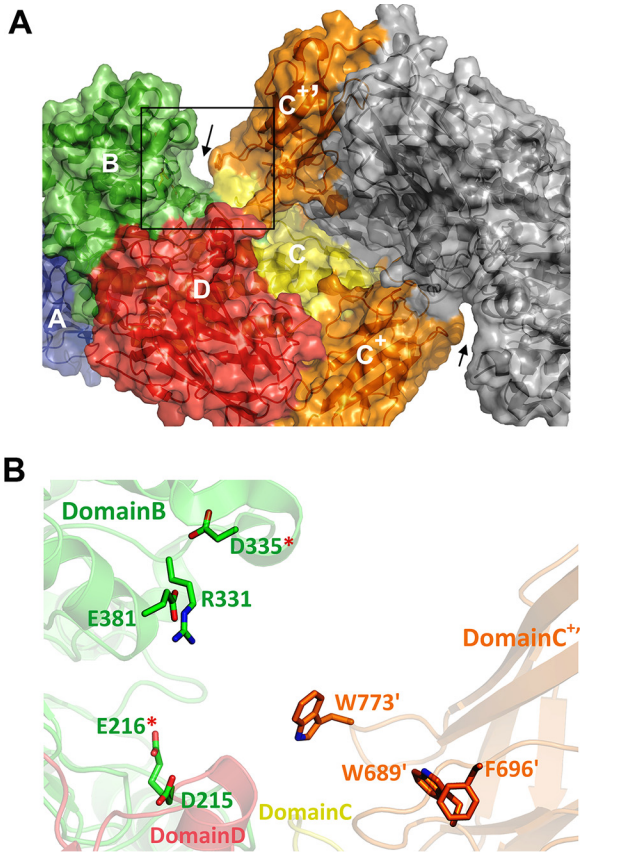

FIGURE 5. **The active site region in SdeAgu115A.** *A*, *surface representation* of the overall structure of SdeAgu115A dimer, with one of the active site regions highlighted by the *rectangular box*. *B*, *close-up* of the highlighted area that is formed by domains B (*green*), C (*yellow*), and D (*red*) from protomer A and domain C^+′ (*orange*) from protomer B. The side chains of the candidate residues tested for their role in catalysis and substrate binding are displayed as *sticks* and *labeled*.

SdeAgu115A, with its domain D positioned adjacent to domain C and a 15-residue loop to link domains C and D (Fig. 3*III*); however, BtGH115A was reported to be a monomer (24). Comparison of the BoAgu115A and BtGH115A structures suggests that the placement of domain D atop domain C blocks access to one side of domain C, thereby limiting the interface available for oligomer formation in BtGH115A. In SdeAgu115A, the insertion of domain C^+ along with the anti-parallel β-sheets formed by residues 667–670 in domain C appeared to reconstitute the interface for stable dimerization of the enzyme.

Site-specific Mutagenesis Highlighted the Role of Individual Residues in Catalysis—In line with previously structurally characterized GH115 enzymes, the active site of SdeAgu115A localized in the large cavity at the C-terminal end of the β/α TIM barrel of the domain B. To probe the essential residues for catalysis, four conserved acidic amino acid residues from domain B (Asp-215, Glu-216, Asp-335, and Glu-381) and one basic arginine residue (Arg-331), were individually replaced by alanine (Fig. 5). In addition to the D335A variant, no activity was detected for the E216A variant of SdeAgu115A (Table 2). CD spectra of SdeAgu115A and its mutants (D335A and E216A) confirmed similar overall structures of the proteins (Fig. 6*A*). Affinity gel electrophoresis was also used to evaluate the impact of mutating Asp-335 and Glu-216 on substrate binding. The

TABLE 2

Kinetic analysis of SdeAgu115A mutant enzymes on beechwood xylan

Kinetic parameters were calculated based on the conventional substrate inhibition equation except for R331A. Values are mean ± S.D. ($n = 3$). ND, no detectable activity.

Enzyme	Residue location	$k_{cat(app)}$	$K_{m(app)}$	$K_{i(app)}$	$k_{cat(app)}/K_{m(app)}$
		s^{-1}	*mg/ml*	*mg/ml*	$s^{-1}\ mg^{-1}\ ml$
Wild type		289 ± 110	43 ± 18	3 ± 1.5	6.7
D215A	Domain B	1 ± 0.1	2 ± 0.5	119 ± 32	0.45
E216A	Domain B	ND	ND	ND	ND
E381A	Domain B	0.3 ± 0.15	12 ± 8	5 ± 3	0.02
D335A	Domain B	ND	ND	ND	ND
R331A	Domain B	0.008 ± 0.001	31 ± 8	—[a]	2.5×10^{-4}
W773A	Domain C^+	129 ± 32	26.4 ± 8.3	19.6 ± 7.5	4.9
W689A	Domain C^+	116 ± 20	12 ± 3	49 ± 20	9.3
F696A	Domain C^+	86 ± 13	13 ± 3	24 ± 6	6.5

[a] Substrate inhibition was not observed for R331A at concentrations of beechwood xylan up to 40 mg/ml; therefore, its data were fitted to the Michaelis-Menten equation.

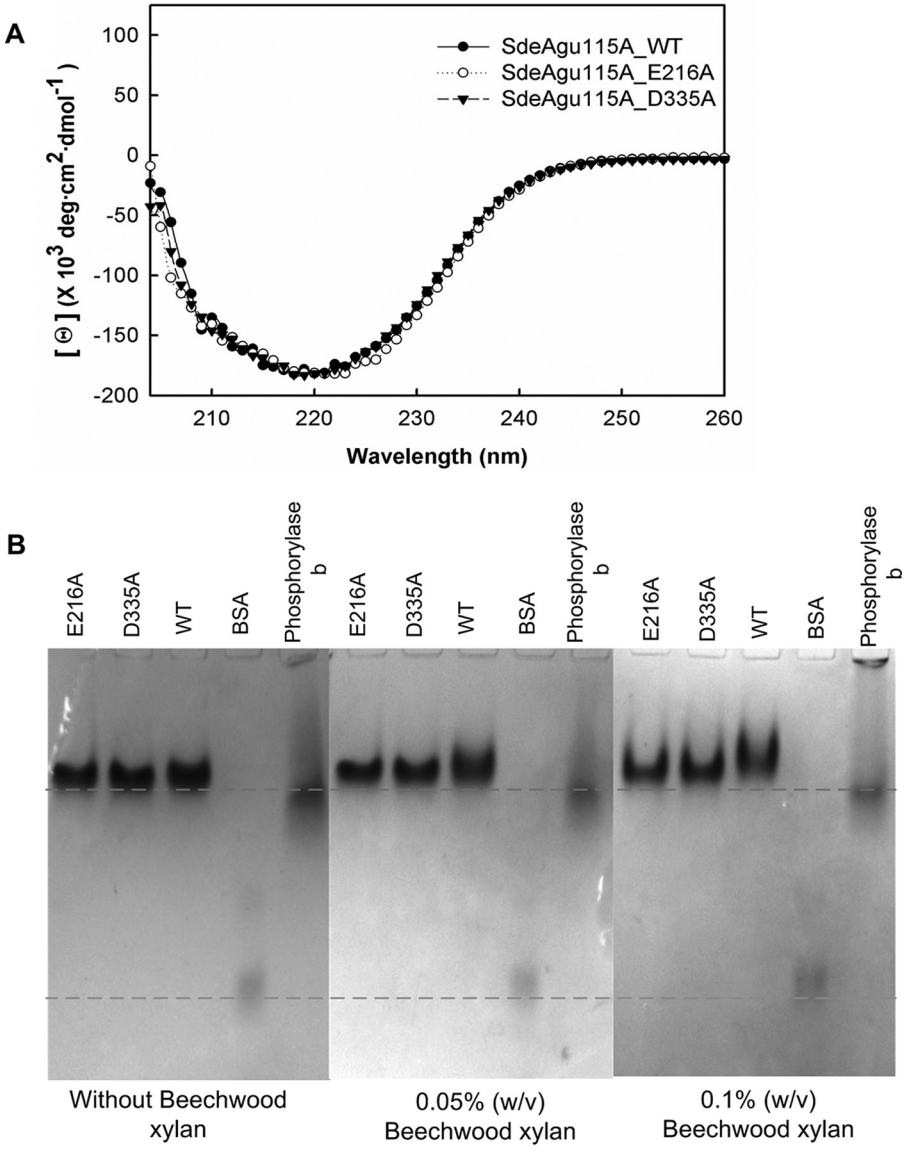

FIGURE 6. **CD spectra and affinity gel electrophoresis analysis of SdeAgu115A and E216A and D335A variants.** *A*, CD spectra of SdeAgu115A along with E216A and D335A variants displayed similar overall structure. *B*, affinity gel electrophoresis analysis with beechwood xylan. The protein band in the *BSA lane* represents the BSA dimer.

slightly slower migration and band smearing observed for the wild-type enzyme and D335A and E216A variants in gels containing beechwood xylan indicated weak binding to the substrate (Fig. 6*B*). Nevertheless, replacing Asp-335 or Glu-216 with alanine appeared to reduce this binding (Fig. 6*B*), suggesting that an activity-associated conformational change may enhance substrate binding by this enzyme. By contrast, D215A and E381A variants remained active, albeit with 15 and 330 times lower catalytic efficiencies, respectively, on beechwood xylan (Table 2). Similar to the R328A mutant of BoAgu115A,

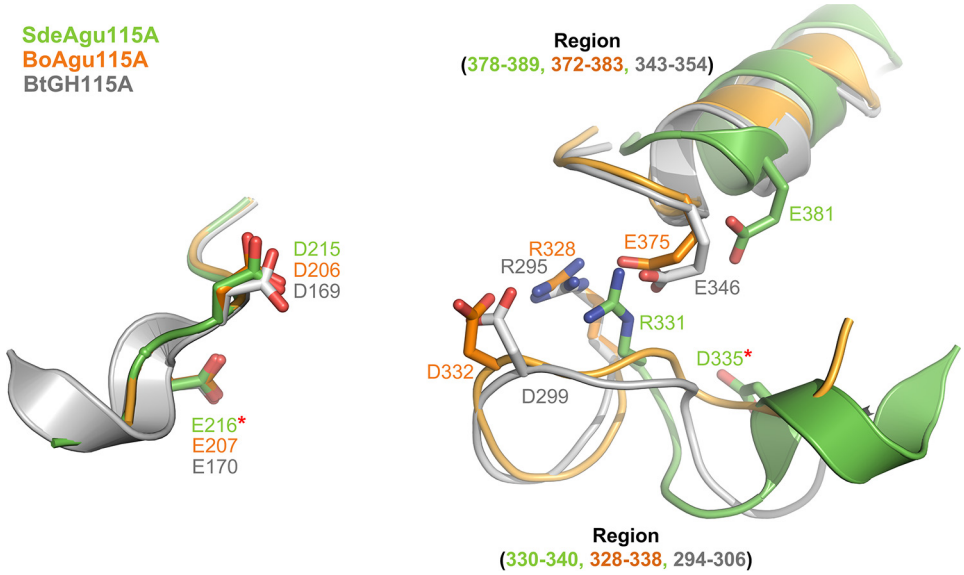

FIGURE 7. **Superimposition of catalytic sites in domain B of SdeAgu115A, BoAgu115A, and BtGH115A.** SdeAgu115A is shown in *green*, BoAgu115A in *orange*, and BtGH115A in *gray*. The identified catalytic essential residues in this study are indicated by *red stars*.

the R331A substitution in SdeAgu115A led to a 26,000-fold decrease in catalytic efficiency, further confirming the importance of this residue for GH115 enzyme activity, probably due to its involvement in positioning and stabilizing the Asp-335 side chain and likely interactions with the carboxylate group in (Me)GlcA*p* as well.

Asp-206, Asp-332, or Glu-375 has been proposed to act as the catalytic acid/base in BoAgu115A (23), whereas these roles were assigned to residues Asp-299 and Glu-346 in BtGH115A (24). However, both E375A and D206A variants of BoAgu115A remained active on beechwood xylan, which is consistent with observations for E381A and D215A variants of SdeAgu115A (Table 2). To date, the catalytic essentiality was biochemically confirmed only for the equivalent residue of Asp-335 in SdeAgu115A (Asp-332 in BoAgu115A). Herein, complete activity loss was also observed for E216A in SdeAgu115A, suggesting its essential role in catalysis. Despite the high conservation of the Glu-216 residue among GH115 enzymes, this residue has not previously been reported as a catalytically important residue (23, 24). Whereas Glu-216 and Asp-335 may represent a catalytic acid/base pair in SdeAgu115A, the distance between Oϵ1 of Glu-216 and Oδ2 of Asp-335 is 22.6 Å (Fig. 5*B*), which is considerably higher than the typical distance of 8–12 Å observed between catalytic residues in other glycosidases that use an inverting mechanism (61). Because these residues are localized to a flexible region, it is possible that their position can change upon substrate binding, as was also proposed for BoAgu115A (23). An overlay of B domains from three available GH115 structures revealed a significant positional shift for Cδ in equivalent residues of Asp-335 in SdeAgu115A (12.6 Å relative to Cδ in Asp-299 of BtGH115, 13.6 Å relative to Asp-332 in BoAgu115A). Comparatively, shifts of equivalent residues to Arg-331 in SdeAgu115A are low, with a distance of 2.5 Å for Cζ relative to Arg-295 in BtGH115A and 3.0 Å relative to Arg-328 in BoAgu115A. These shifts can be explained by movement in the loop formed by residues 330–340 in SdeAgu115A (Fig. 7). Unfortunately, attempts to obtain the SdeAgu115A-GlcA*p* complex structure to further clarify involvement of specific residues in catalysis and substrate binding were unsuccessful (see "Experimental Procedures" for details).

Domain C$^+$ Participated in Xylan Substrate Binding—Further analysis of domain B in SdeAgu115A revealed a long and deep cleft above and flanking the active site cavity, which could accommodate the backbone of xylan substrates. Notably, this cleft further extended into domain D of the same SdeAgu115A monomer (Fig. 5*A*). By contrast, the predicted xylan-binding cleft of BoAgu115A was formed by domain B and the C-terminal domain D′ of the neighboring protomer (23).

Two loop regions spanning residues 689–696 and 770–775 in the additional C$^+$′ domain of SdeAgu115A extended the sides of the xylan binding cleft, increasing its depth (Fig. 5*A*). To assess the potential role of these two loop regions in substrate binding, three aromatic residues (Trp-773, Trp-689, and Phe-696) within these loops were individually mutated to alanine, and their activities were evaluated. Although k_{cat} values of all three mutants (W773A, W689A, and F696A) was decreased by 3–5 times compared with the wild type, these mutants displayed catalytic efficiency on beechwood xylan similar to that of the wild type enzyme due to slightly decreased $K_{m(app)}$ values (Table 2). All three mutants also displayed reduced substrate inhibition with increased $K_{i(app)}$ values, particularly for W689A, where the $K_{i(app)}$ was increased by 15 times relative to wild type. The reduction in $K_{m(app)}$ values observed for each of the W773A, W689A, and F696A mutants was at first surprising given the presumed role of these aromatic residues in substrate stacking. However, the relative stability of the α-(1→2) linkage between MeGlcA*p* and Xyl*p* compared with β-(1→4)-D-Xyl*p* backbone linkages is well recognized (62). It is conceivable, then, that the aromatic residues present in loop regions of the additional domain C$^+$ increase torsional strain within the bound substrate, thus decreasing the stability of the targeted glycosidic linkage.

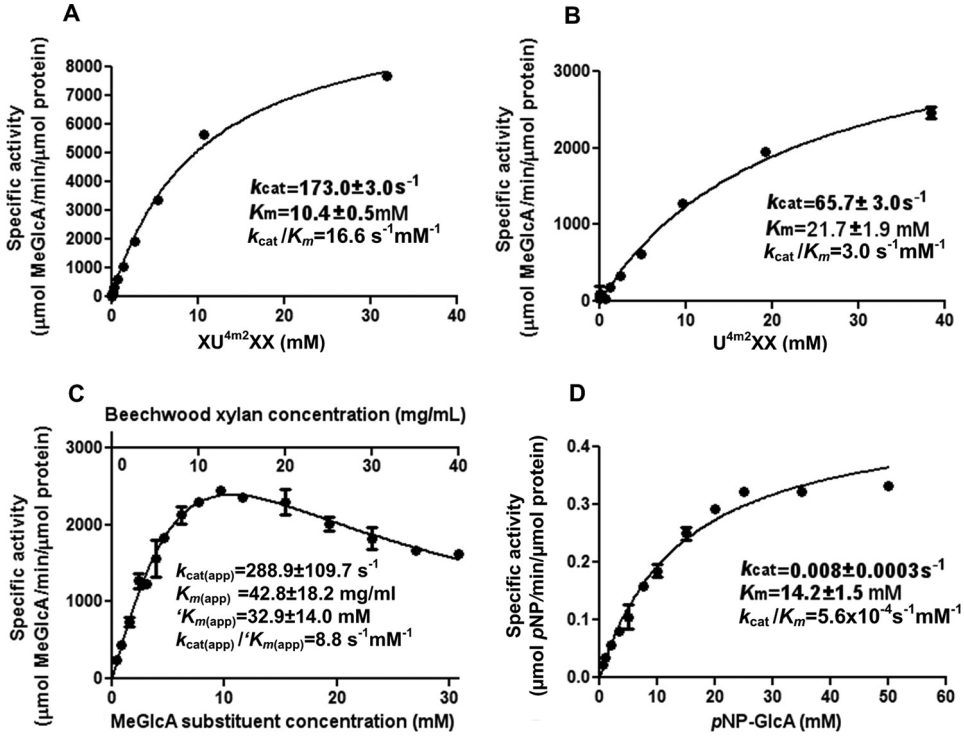

FIGURE 8. **Kinetic parameters of SdeAgu115A on selected substrates: XU^{4m2}XX (*A*), U^{4m2}XX (*B*), beechwood xylan (*C*), and *p*NP-GlcA*p* (*D*).** Data corresponding to *A*, *B*, and *D* were fitted to the Michaelis-Menten equation. Activity data collected using beechwood xylan were fitted to a conventional substrate inhibition equation. The normalized concentration of the MeGlcA*p* in the glucuronoxylan (mM) is presented as $k_{m(app)}$. *Error bars*, S.D.

Implications of SdeAgu115A Structure on Its Substrate Profile—The glucurono-xylooligosaccharides were generated with a yield >10% (w/w); their purity (over 98%) was confirmed by TLC, high performance anion exchange chromatography with pulsed amperometric detection, and electrospray ionization-MS. The activity (k_{cat}) of SdeAgu115A on XU^{4m2}XX and U^{4m2}XX was 173.3 ± 3.0 and 65.7 ± 3.0 s^{-1}, respectively (Fig. 8), indicating that the enzyme was active on both terminal and internal MeGlcA*p* substitutions. Furthermore, SdeAgu115A revealed a catalytic efficiency (k_{cat}/K_m) of 16.6 s^{-1} mM^{-1} for XU^{4m2}XX, which is 5.5 times higher than that of U^{4m2}XX (3.0 s^{-1} mM^{-1}) (Fig. 8). The comparatively high catalytic efficiency measured using XU^{4m2}XX was explained by both a 2.6-fold increase in k_{cat} and a 2.1-fold decrease in K_m compared with the value obtained using U^{4m2}XX. A similar pattern was reported for BoAgu115A (23) and suggests that, as in BoAgu115A, at least one subsite (+2NR) beyond the +1 subsite of SdeAgu115A participates in xylan backbone binding.

Among the xylan substrates, SdeAgu115A showed the highest activity toward beechwood glucuronoxylan, followed by spruce arabinoglucuronoxylan and oat spelt xylan (Table 3). This is the first report directly comparing GH115 specific activity on hardwood, softwood, and cereal xylans. Beechwood glucuronoxylan comprises a β-(1→4)-Xyl*p* backbone substituted with α-(1→2)-MeGlcA*p*, where the ratio of Xyl*p* to MeGlcA*p* is ~8:1 (3) (Fig. 9). Similarly, the β-(1→4)-Xyl*p* backbone of spruce arabinoglucuronoxylan and oat spelt xylan is decorated by α-(1→2)-MeGlcA*p*; however, these xylans are further substituted by Ara*f*, where the ratio of MeGlcA*p* to Ara*f*: Xyl*p* in spruce arabinoglucuronoxylan and oat spelt xylan is ~2:1:11 and 1:3:24, respectively (32, 64). The lower activity of SdeAgu115A toward oat spelt xylan could be explained by the comparatively low water solubility of this substrate preparation, which would lower the effective MeGlcA*p* content available to the enzyme. Lower activity toward spruce arabinoglucuronoxylan was more difficult to explain, given the comparatively high water solubility of this substrate and the 1.5-fold higher MeGlcA*p* content compared with beechwood xylan. Previous studies of GH115 α-glucuronidase using acetylated glucurono-xylooligosaccharides demonstrate that although GH115 enzymes can access (Me)GlcA*p* substituents from internal regions of xylan, they may be restricted to singly substituted Xyl*p* residues (16). Analogously, it could be that lower activity of SdeAgu115A on spruce arabinoglucuronoxylan is due to partial obstruction by Ara*f* residues despite its position on other Xyl*p* units, which would further support the formation of an extended substrate binding site by this and potentially other GH115 enzymes.

TABLE 3

Activity profile of SdeAgu115A

The final concentration of substrates in activity assay solution was 1% (w/v). No activity was detected toward alginate, rhamnogalacturonan, apple pectin, and gum arabic. Values shown are mean ± S.D. (n = 3). Infusion negative ion spectra confirmed that only MeGlcA*p* (*m/z* 207) was released from beechwood xylan by SdeAgu115A (data not shown).

Polymeric substrates	Activity	Relative activity[a]
	μmol product/min/μmol enzyme	%
Beechwood xylan	2470 ± 72	100 ± 2.9
Spruce arabinoglucuronoxylan	917 ± 6	37 ± 0.2
Oat spelt xylan	24 ± 1	1.0 ± 0.04

[a] Relative activity was calculated based on maximum activity values for each substrate category.

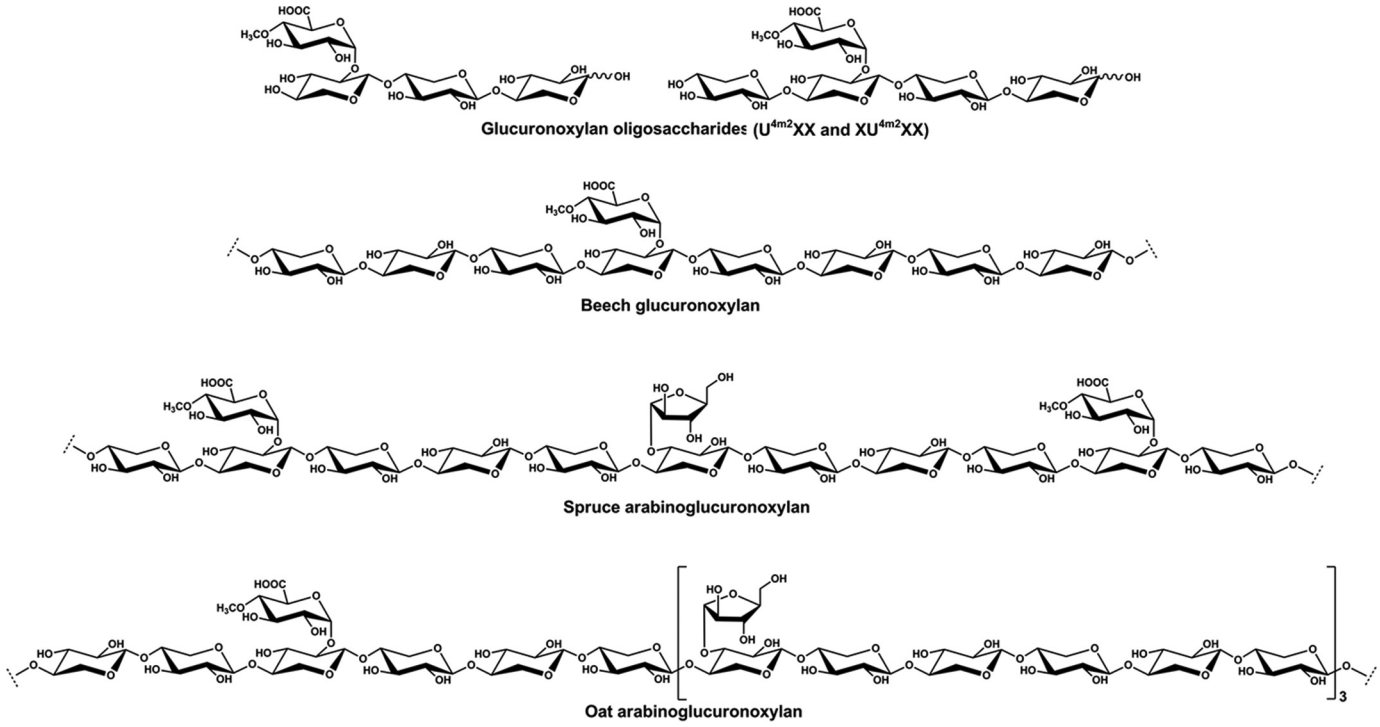

FIGURE 9. **Schematic structures of xylan substrates used in activity studies of SdeAgu115A.**

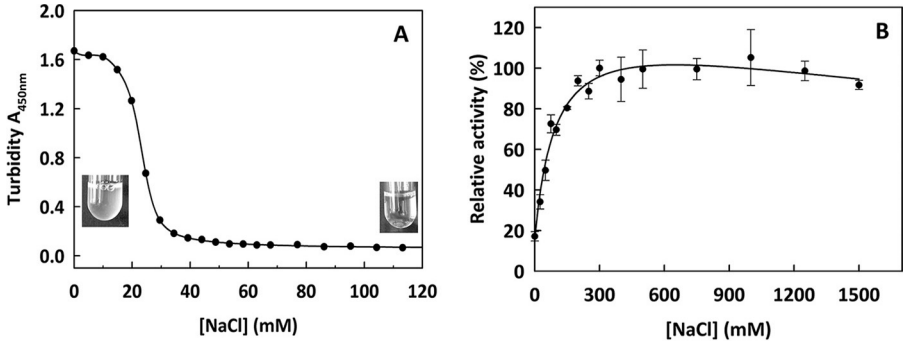

FIGURE 10. **The effect of NaCl to SdeAgu115A reversible aggregation and its activity on beechwood xylan.** *A*, dialysis of enzyme solution against 20 mM Hepes buffer (pH 7.0) led to protein aggregation; turbidity at $A_{450\,nm}$ decreased through titration with NaCl. *B*, the Nelson-Somogyi method was used to measure SdeAgu115A activity in 100 mM MES buffer (pH 6.5) containing different NaCl concentrations. Full relative activity (100%) was obtained at 300 mM NaCl. *Error bars*, S.D.

SdeAgu115A displayed low but detectable activity toward *p*NP-GlcA*p* (Fig. 8), which has not been tested for GH67 and other GH115 enzymes characterized to date. Still, k_{cat} values obtained using *p*NP-GlcA*p* were 8200–36,000 times lower than apparent k_{cat} values obtained using glucurono-xylooligosaccharides and beechwood xylan (Fig. 8), underscoring the critical importance of including non-synthetic substrates in screens for new enzyme activity. Kinetic analyses also revealed substrate inhibition of SdeAgu115A by beechwood xylan (Fig. 8*C*), suggesting the non-catalytic interactions between SdeAgu115A and this substrate. Substrate inhibition can be caused by the non-productive binding of substrate molecules to different subsites within the enzyme substrate binding site (65). Thus, the substrate inhibition observed for SdeAgu115A implies a multisubsite binding cleft at the surface of this enzyme. Notably, substrate inhibition has not been reported for other GH115 enzymes characterized to date.

Impact of NaCl on the Aggregation and Activity of SdeAgu115A—SdeAgu115A was observed to aggregate in 20 mM HEPES buffer (pH 7.0). The aggregation was reversed by adding NaCl up to 40 mM in 20 mM HEPES buffer (pH 7.5) (Fig. 10*A*). Interestingly, the presence of NaCl (up to 300 mM) enhanced SdeAgu115A activity toward beechwood xylan up to 6-fold. Moreover, 80% of SdeAgu115A activity was retained in 1.5 M NaCl (Fig. 10*B*). NaCl tolerance and activation have been reported for several enzymes from other marine bacteria (52, 63). Altogether, it was consistent with the marine habitat of the enzyme source organism.

Conclusion—Only a few α-glucuronidases from family GH115 have been characterized to date. Two recently published GH115 structures both exhibited four-domain architectures. Herein, we present a GH115 α-glucuronidase (SdeAgu115A) from the marine bacterium *S. degradans* 2-40^T with a novel five-domain architecture, which will be shared by more than

half of GH115 members. The domain C^+ insertion in SdeAgu115A significantly impacted domain arrangement and its dimerization, which is the predominant functional oligomeric state of this enzyme. In addition, an essential catalytic residue, Glu-216 in SdeAgu115A, was identified for the first time in a GH115 enzyme. Furthermore, site-specific mutagenesis revealed the participation of the C^+ domain in xylan substrate binding and the benefit of altering the C^+ region to modulate substrate inhibition. These results may benefit efforts to minimize detrimental impacts of Ara*f* and acetyl substitutions on GH115 action through protein engineering. Determination of high resolution complex structures of SdeAgu115A in complex with ligands will be key to further evaluating these possibilities.

Author Contributions—E. R. M. and A. S. conceived and coordinated the study; W. W., R. Y., B. P. N., T. V. V., R. D. L., X. X., H. C., M. T., P. G., and G. T. conducted the experiments; P. G. and G. T. prepared the spruce arabinoglucuronoxylan used in the study; and W. W., R. Y., B. P. N., A. S., and E. R. M. wrote the paper. All authors reviewed the results and approved the final version of the manuscript.

Acknowledgments—We thank G. Brown and Professor A. Yakunin (University of Toronto) for technical support and Dr. Masoud Vedadi and Dr. Guillermo Senisterra (Structural Genomics Consortium, Toronto, Canada) for circular dichroism spectra acquisition. We also thank K. Parikka for preparing figures of xylan structures. Structural results shown in this report are derived from work performed at Argonne National Laboratory, Structural Biology Center at the Advanced Photon Source. Argonne National Laboratory is operated by UChicago Argonne, LLC, for the United States Department of Energy, Office of Biological and Environmental Research, under contract DE-AC02-06CH11357.

References

1. Busse-Wicher, M., Gomes, T. C., Tryfona, T., Nikolovski, N., Stott, K., Grantham, N. J., Bolam, D. N., Skaf, M. S., and Dupree, P. (2014) The pattern of xylan acetylation suggests xylan may interact with cellulose microfibrils as a twofold felical screw in the secondary plant cell wall of *Arabidopsis thaliana*. *Plant J.* **79,** 492–506
2. Scheller, H. V., and Ulvskov, P. (2010) Hemicelluloses. *Annu. Rev. Plant Biol.* **61,** 263–289
3. Teleman, A., Lundqvist, J., Tjerneld, F., Stålbrand, H., and Dahlman, O. (2000) Characterization of acetylated 4-O-methylglucuronoxylan isolated from aspen employing 1H and 13C NMR spectroscopy. *Carbohydr. Res.* **329,** 807–815
4. Timell, T. (1967) Recent progress in the chemistry of wood hemicelluloses. *Wood Sci. Technol.* **1,** 45–70
5. Shallom, D., and Shoham, Y. (2003) Microbial hemicellulases. *Curr. Opin. Microbiol.* **6,** 219–228
6. de Vries, R. P., Kester, H. C., Poulsen, C. H., Benen, J. A., and Visser, J. (2000) Synergy between enzymes from *Aspergillus* involved in the degradation of plant cell wall polysaccharides. *Carbohydr. Res.* **327,** 401–410
7. Coughlan, M. P., and Hazlewood, G. P. (1993) β-1,4-D-Xylan-degrading enzyme systems: biochemistry, molecular biology and applications. *Biotechnol. Appl. Biochem.* **17**, 259–289
8. Gilbert, H. J., Stålbrand, H., and Brumer, H. (2008) How the walls come crumbling down: recent structural biochemistry of plant polysaccharide degradation. *Curr. Opin. Plant Biol.* **11,** 338–348
9. Bosmans, T. J., Stépán, A. M., Toriz, G., Renneckar, S., Karabulut, E., Wågberg, L., and Gatenholm, P. (2014) Assembly of debranched xylan from solution and on nanocellulosic surfaces. *Biomacromolecules* **15,** 924–930
10. Mikkonen, K. S., and Tenkanen, M. (2012) Sustainable food-packaging materials based on future biorefinery products: xylans and mannans. *Trends Food Sci. Technol.* **28,** 90–102
11. Sedlmeyer, F. B. (2011) Xylan as by-product of biorefineries: characteristics and potential use for food applications. *Food Hydrocoll.* **25,** 1891–1898
12. Henrissat, B. (1991) A classification of glycosyl hydrolases based sequence similarities amino acid. *Biochem. J.* **280,** 309–316
13. Suresh, C., Kitaoka, M., and Hayashi, K. (2003) A thermostable non-xylanolytic α-glucuronidase of *Thermotoga maritima* MSB8. *Biosci. Biotechnol. Biochem.* **67,** 2359–2364
14. Suresh, C., Rus'd, A. A., Kitaoka, M., and Hayashi, K. (2002) Evidence that the putative α-glucosidase of *Thermotoga maritima* MSB8 is a pNP α-D-glucuronopyranoside hydrolyzing α-glucuronidase. *FEBS Lett.* **517,** 159–162
15. Bronnenmeier, K., Meissner, H., Stocker, S., and Staudenbauer, W. L. (1995) α-D-Glucuronidases from the xylanolytic thermophiles *Clostridium stercorarium* and *Thermoanaerobacterium saccharolyticum*. *Microbiology* **141,** 2033–2040
16. Tenkanen, M., and Siika-aho, M. (2000) An α-glucuronidase of *Schizophyllum commune* acting on polymeric xylan. *J. Biotechnol.* **78,** 149–161
17. Ryabova, O., Vrsanská, M., Kaneko, S., van Zyl, W. H., and Biely, P. (2009) A novel family of hemicellulolytic α-glucuronidase. *FEBS Lett.* **583,** 1457–1462
18. Biely, P., de Vries, R. P., Vrsanská, M., and Visser, J. (2000) Inverting character of α-glucuronidase A from *Aspergillus tubingensis*. *Biochim. Biophys. Acta* **1474,** 360–364
19. Rosa, L., Ravanal, M. C., Mardones, W., and Eyzaguirre, J. (2013) Characterization of a recombinant α-glucuronidase from *Aspergillus fumigatus*. *Fungal Biol.* **117,** 380–387
20. Golan, G., Shallom, D., Teplitsky, A., Zaide, G., Shulami, S., Baasov, T., Stojanoff, V., Thompson, A., Shoham, Y., and Shoham, G. (2004) Crystal structures of *Geobacillus stearothermophilus* α-glucuronidase complexed with its substrate and products: mechanistic implications. *J. Biol. Chem.* **279,** 3014–3024
21. Nurizzo, D., Nagy, T., Gilbert, H. J., and Davies, G. J. (2002) The structural basis for catalysis and specificity of the *Pseudomonas cellulosa* α-glucuronidase, GlcA67A. *Structure* **10,** 547–556
22. Chong, S.-L., Battaglia, E., Coutinho, P. M., Henrissat, B., Tenkanen, M., and de Vries, R. P. (2011) The α-glucuronidase Agu1 from *Schizophyllum commune* is a member of a novel glycoside hydrolase family (GH115). *Appl. Microbiol. Biotechnol.* **90,** 1323–1332
23. Rogowski, A., Baslé, A., Farinas, C. S., Solovyova, A., Mortimer, J. C., Dupree, P., Gilbert, H. J., and Bolam, D. N. (2014) Evidence that GH115 α-glucuronidase activity, which is required to degrade plant biomass, is dependent on conformational flexibility. *J. Biol. Chem.* **289,** 53–64
24. Aalbers, F., Turkenburg, J. P., Davies, G. J., Dijkhuizen, L., and Lammerts van Bueren, A. (2015) Structural and functional characterization of a novel family GH115 4-*O*-methyl-α-glucuronidase with specificity for decorated arabinogalactans. *J. Mol. Biol.* **427,** 3935–3946
25. Fujimoto, Z., Ichinose, H., Biely, P., and Kaneko, S. (2011) Crystallization and preliminary crystallographic analysis of the glycoside hydrolase family 115 α-glucuronidase from *Streptomyces pristinaespiralis*. *Acta Crystallogr. Sect. F Struct. Biol. Cryst. Commun.* **67,** 68–71
26. Kolenová, K., Ryabova, O., Vrsanská, M., and Biely, P. (2010) Inverting character of family GH115 α-glucuronidases. *FEBS Lett.* **584,** 4063–4068
27. Andrykovitch, G., and Marx, I. (1988) Isolation of a new polysaccharide-digesting bacterium from a salt marsh. *Appl. Environ. Microbiol.* **54,** 1061–1062
28. Ekborg, N. A., Taylor, L. E., Longmire, A. G., Henrissat, B., Weiner, R. M., and Hutcheson, S. W. (2006) Genomic and proteomic analyses of the agarolytic system expressed by *Saccharophagus degradans* 2-40. *Appl. Environ. Microbiol.* **72,** 3396–3405
29. Taylor, L. E., 2nd, Henrissat, B., Coutinho, P. M., Ekborg, N. A., Hutcheson, S. W., and Weiner, R. M. (2006) Complete cellulase system in the marine bacterium *Saccharophagus degradans* strain 2-40T. *J. Bacteriol.* **188,** 3849–3861
30. Weiner, R. M., Taylor, L. E., 2nd, Henrissat, B., Hauser, L., Land, M.,

Coutinho, P. M., Rancurel, C., Saunders, E. H., Longmire, A. G., Zhang, H., Bayer, E. A., Gilbert, H. J., Larimer, F., Zhulin, I. B., Ekborg, N. A., *et al.* (2008) Complete genome sequence of the complex carbohydrate-degrading marine bacterium, *Saccharophagus degradans* strain 2-40 T. *PLoS Genet.* **4,** e1000087

31. Hutcheson, S. W., Zhang, H., and Suvorov, M. (2011) Carbohydrase systems of *Saccharophagus degradans* degrading marine complex polysaccharides. *Mar. Drugs* **9,** 645–665
32. Escalante, A., Gonçalves, A., Bodin, A., Stepan, A., Sandström, C., Toriz, G., and Gatenholm, P. (2012) Flexible oxygen barrier films from spruce xylan. *Carbohydr. Polym.* **87,** 2381–2387
33. Liu, H., and Naismith, J. H. (2008) An efficient one-step site-directed deletion, insertion, single and multiple-site plasmid mutagenesis protocol. *BMC Biotechnol.* **8,** 91
34. Bradford, M. M. (1976) A rapid and sensitive method for the quantitation of microgram quantities of protein utilizing the principle of protein-dye binding. *Anal. Biochem.* **72,** 248–254
35. Laemmli, U. K. (1970) Cleavage of structural proteins during the assembly of the head of bacteriophage T4. *Nature* **227,** 680–685
36. DuBois, M., Gilles, K. A., Hamilton, J. K., Rebers, P. A., and Smith, F. (1956) Colorimetric method for determination of sugars and related substances. *Anal. Chem.* **28,** 350–356
37. Koutaniemi, S., Guillon, F., Tranquet, O., Bouchet, B., Tuomainen, P., Virkki, L., Petersen, H. L., Willats, W. G. T., Saulnier, L., and Tenkanen, M. (2012) Substituent-specific antibody against glucuronoxylan reveals close association of glucuronic acid and acetyl substituents and distinct labeling patterns in tree species. *Planta* **236,** 739–751
38. Vuong, T. V., Vesterinen, A.-H., Foumani, M., Juvonen, M., Seppälä, J., Tenkanen, M., and Master, E. R. (2013) Xylo- and cello-oligosaccharide oxidation by gluco-oligosaccharide oxidase from *Sarocladium strictum* and variants with reduced substrate inhibition. *Biotechnol. Biofuels.* **6,** 148
39. Smogyi, M. (1952) Notes on sugar determination. *J. Biol. Chem.* **195,** 19–23
40. Laue, T. M., Shah, B. D., Ridgeway, T. M., and Pelletier, S. M. (1992) Computer-aided interpretation of analytical sedimentation data for proteins. in *Analytical Ultracentrifugation in Biochemistry and Polymer Science* (Harding, S. E., Rowe, A. J., and Horton, J. C., eds) pp. 90–125, Royal Society of Chemistry, London
41. Freelove, A. C. J., Bolam, D. N., White, P., Hazlewood, G. P., and Gilbert, H. J. (2001) A novel carbohydrate-binding protein is a component of the plant cell wall-degrading complex of *Piromyces equi*. *J. Biol. Chem.* **276,** 43010–43017
42. Nocek, B., Mulligan, R., Bargassa, M., Collart, F., and Joachimiak, A. (2008) Crystal structure of aminopeptidase N from human pathogen *Neisseria meningitidis*. *Proteins* **70,** 273–279
43. Rosenbaum, G., Alkire, R. W., Evans, G., Rotella, F. J., Lazarski, K., Zhang, R. G., Ginell, S. L., Duke, N., Naday, I., Lazarz, J., Molitsky, M. J., Keefe, L., Gonczy, J., Rock, L., Sanishvili, R., *et al.* (2006) The Structural Biology Center 19ID undulator beamline: facility specifications and protein crystallographic results. *J. Synchrotron Radiat.* **13,** 30–45
44. Minor, W., Cymborowski, M., Otwinowski, Z., and Chruszcz, M. (2006) HKL-3000: The integration of data reduction and structure solution: from diffraction images to an initial model in minutes. *Acta Crystallogr. D Biol. Crystallogr.* **62,** 859–866
45. Collaborative Computational Project, Number 4 (1994) The CCP4 suite: programs for protein crystallography. *Acta Crystallogr. D Biol. Crystallogr.* **50,** 760–763
46. Terwilliger, T. C., and Berendzen, J. (1999) Automated MAD and MIR structure solution. *Acta Crystallogr. D Biol. Crystallogr.* **55,** 849–861
47. Terwilliger, T. (2004) SOLVE and RESOLVE: automated structure solution, density modification, and model building. *J. Synchrotron Radiat.* **11,** 49–52
48. Cowtan, K. (2001) Fast Fourier feature recognition. *Acta Crystallogr. D Biol. Crystallogr.* **57,** 1435–1444
49. Sheldrick, G. M. (2002) Macromolecular phasing with SHELXE. *Z. Kristallogr.* **217,** 644–650
50. Cowtan, K., and Main, P. (1998) Miscellaneous algorithms for density modification. *Acta Crystallogr. D Biol. Crystallogr.* **54,** 487–493
51. Cowtan, K. D., and Zhang, K. Y. (1999) Density modification for macromolecular phase improvement. *Prog. Biophys. Mol. Biol.* **72,** 245–270
52. Uchimura, K., Miyazaki, M., Nogi, Y., Kobayashi, T., and Horikoshi, K. (2010) Cloning and sequencing of alginate lyase genes from deep-sea strains of *Vibrio* and *Agarivorans* and characterization of a new *Vibrio* enzyme. *Mar. Biotechnol.* **12,** 526–533
53. Pathak, S., Dorfmueller, H. C., Borodkin, V. S., and van Aalten, D. M. F. (2008) Chemical dissection of the link between streptozotocin, *O*-GlcNAc, and pancreatic cell death. *Chem. Biol.* **15,** 799–807
54. Ito, T., Katayama, T., Hattie, M., Sakurama, H., Wada, J., Suzuki, R., Ashida, H., Wakagi, T., Yamamoto, K., Stubbs, K. A., and Fushinobu, S. (2013) Crystal structures of a glycoside hydrolase family 20 lacto-*N*-biosidase from *Bifidobacterium bifidum*. *J. Biol. Chem.* **288,** 11795–11806
55. Holm, L., and Rosenström, P. (2010) Dali server: conservation mapping in 3D. *Nucleic Acids Res.* **38,** W545–W549
56. Knight, S. D., Choudhury, D., Hultgren, S., Pinkner, J., Stojanoff, V., and Thompson, A. (2002) Structure of the S pilus periplasmic chaperone SfaE at 2.2 Å resolution. *Acta Crystallogr. D Biol. Crystallogr.* **58,** 1016–1022
57. Eidam, O., Dworkowski, F. S. N., Glockshuber, R., Grütter, M. G., and Capitani, G. (2008) Crystal structure of the ternary FimC-FimFt-FimDN complex indicates conserved pilus chaperone-subunit complex recognition by the usher FimD. *FEBS Lett.* **582,** 651–655
58. Larsbrink, J., Rogers, T. E., Hemsworth, G. R., McKee, L. S., Tauzin, A. S., Spadiut, O., Klinter, S., Pudlo, N. A., Urs, K., Koropatkin, N. M., Creagh, A. L., Haynes, C. A., Kelly, A. G., Cederholm, S. N., Davies, G. J., *et al.* (2014) A discrete genetic locus confers xyloglucan metabolism in select human gut Bacteroidetes. *Nature* **506,** 498–502
59. Mello, L. V., Chen, X., and Rigden, D. J. (2010) Mining metagenomic data for novel domains: BACON, a new carbohydrate-binding module. *FEBS Lett.* **584,** 2421–2426
60. de Beer, T. A. P., Berka, K., Thornton, J. M., and Laskowski, R. A. (2014) PDBsum additions. *Nucleic Acids Res.* **42,** D292–D296
61. Rye, C. S., and Withers, S. G. (2000) Glycosidase mechanisms. *Curr. Opin. Chem. Biol.* **4,** 573–580
62. De Ruiter, G. A., Schols, H. A., Voragen, A. G. J., and Rombouts, F. M. (1992) Carbohydrate analysis of water-soluble uronic acid-containing polysaccharides with high-performance anion-exchange chromatography using methanolysis combined with TFA hydrolysis is superior to four other methods. *Anal. Biochem.* **207,** 176–185
63. Lemak, S., Tchigvintsev, A., Petit, P., Flick, R., Singer, A. U., Brown, G., Evdokimova, E., Egorova, O., Gonzalez, C. F., Chernikova, T. N., Yakimov, M. M., Kube, M., Reinhardt, R., Golyshin, P. N., Savchenko, A., and Yakunin, A. F. (2012) Structure and activity of the cold-active and anion-activated carboxyl esterase OLEI01171 from the oil-degrading marine bacterium *Oleispira antarctica*. *Biochem. J.* **445,** 193–203
64. Kormelink, F. J. M., and Voragen, A. G. J. (1993) Degradation of different [(glucurono)arabino]xylans by a combination of purified xylan-degrading enzymes. *Appl. Microbiol. Biotechnol.* **38,** 688–695
65. Copeland, R. A. (2000) *Enzymes: A Practical Introduction to Structure, Mechanism, and Data Analysis*, pp. 109–145, Wiley-VCH, Weinheim, Germany